TU Delft

Delft University of Technology

Document Version
Final published version

Licence
CC BY

Citation (APA)
Feije, L. J., Timmer, G. M., Karababa, R., van de Stolpe, G. L., Martens, T., Loenen, S. J. H., Durant, T. B. A., Das, A., Taminiau, T. H., & More Authors (2026). Laser-Induced Creation of Coherent V2 Centers in Bulk-Grown Silicon Carbide. *Nano Letters*, *26*(28), 9143-9150. https://doi.org/10.1021/acs.nanolett.6c01807

Important note
To cite this publication, please use the final published version (if applicable).
Please check the document version above.

Copyright
In case the licence states “Dutch Copyright Act (Article 25fa)”, this publication was made available Green Open Access via the TU Delft Institutional Repository pursuant to Dutch Copyright Act (Article 25fa, the Taverne amendment). This provision does not affect copyright ownership.
Unless copyright is transferred by contract or statute, it remains with the copyright holder.

Sharing and reuse
Other than for strictly personal use, it is not permitted to download, forward or distribute the text or part of it, without the consent of the author(s) and/or copyright holder(s), unless the work is under an open content license such as Creative Commons.

Takedown policy
Please contact us and provide details if you believe this document breaches copyrights.
We will remove access to the work immediately and investigate your claim.

This work is downloaded from Delft University of Technology.

NANO LETTERS

Open Access
This article is licensed under CC-BY 4.0

pubs.acs.org/NanoLett
Letter

Laser-Induced Creation of Coherent V2 Centers in Bulk-Grown Silicon Carbide

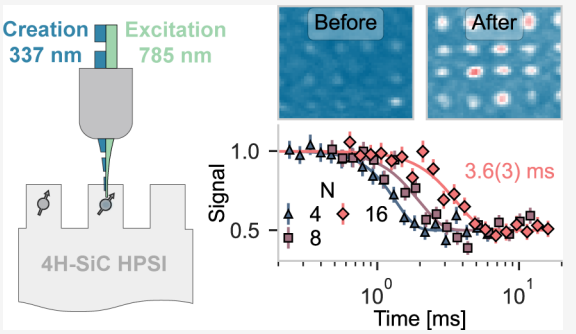
Laurens J. Feije,[‖] Gerben M. Timmer,[‖] Yihong Hu, Rana Karababa, Guido L. van de Stolpe, Tobias Martens, Sjoerd J. H. Loenen, Theo B. A. Durant, Antariksha Das, Aaron M. Day, Evelyn L. Hu, and Tim H. Taminiau*

Cite This: *Nano Lett.* 2026, 26, 9143−9150

Read Online

ACCESS | Metrics & More | Article Recommendations | Supporting Information

ABSTRACT: Solid-state spin defects are promising qubits for quantum network nodes. A key challenge toward larger networks is creating defects with high yield into nanophotonic devices while maintaining good optical and spin properties. Here, we demonstrate the creation of single V2 centers in nanopillars fabricated from commercial bulk-grown 4H-silicon carbide using a pulsed above-bandgap (UV) laser. We observe an 11-fold increase in the V2 center occurrence after UV laser illumination. These laser-induced V2 centers exhibit narrow optical line widths and spectral diffusion rates comparable to naturally occurring V2 centers in nanopillars of the same material. Furthermore, we measure a spin coherence time of $T_2^{DD} = 3.6(3)$ ms under dynamical decoupling, consistent with dephasing by the nuclear-spin bath. This demonstration of the in situ, postfabrication generation of coherent V2 centers in nanostructures in widely available bulk-grown 4H-SiC shows the potential for above-bandgap laser illumination for scalable defect creation in integrated photonic devices.



KEYWORDS: *Color centers, Laser-induced defect creation, Nanophotonic structures, Silicon carbide, Quantum networks, Solid-state qubits*

Solid-state spin defects provide promising qubits for quantum networks, as they combine high-fidelity spin-photon entanglement with access to nuclear spins with long coherence times.[1−3] Their compatibility with integrated photonics offers a scalable path toward large-scale quantum networks.[4−6] A central challenge is the deterministic placement of defects within subwavelength nanophotonic structures while preserving good optical and spin coherence.[7−10]

Silicon carbide (4H-SiC) hosts a variety of optically active spin defects, including silicon vacancies, divacancies, the vanadium defect and the NV center.[10−20] The negatively charged single k-site silicon vacancy center (V2) is a promising candidate as long spin coherence times and near-lifetime-limited optical transitions, required for remote entanglement generation, have been demonstrated in nanophotonic devices.[21−23]

Several methods have successfully demonstrated the creation of localized single V2 centers, such as masked He^+ ion implantation, which has been shown to yield V2 centers with good optical and spin coherence,[21,24] and focused ion beam (FIB) implantation,[25−27] including with in situ monitoring.[28] Pulsed-laser writing is a compelling alternative that provides defect creation with good spatial precision, typically on the order of 100−200 nm, after device fabrication.[29−32] In addition, laser writing is compatible with in situ monitoring,[29] potentially enabling deterministic defect creation. Pioneering experiments in 4H-SiC have shown that below-bandgap laser writing can create color centers in bulk,[31−33] while above-bandgap laser writing has further enabled the creation of V2 centers in 1D nanophotonic crystal cavities.[30]

However, the optical and spin coherence of single laser-written defects in 4H-SiC, which are essential for many quantum applications, have thus far remained unexplored.

Here, we demonstrate laser-induced creation of V2 centers in nanopillars with preserved optical and spin coherence. We use an above-bandgap laser and commercial bulk-grown high-purity semi-insulating (HPSI) 4H-SiC, widely available as 4−6 in. wafers.

We first identify the pulse energy window that enables defect formation without inducing surface amorphization. Subsequently, we show the creation of single laser-induced V2 centers and characterize their optical properties. We show near-lifetime-limited optical line widths and slow spectral diffusion rates, similar to naturally occurring V2 centers in the

Received: April 15, 2026
Revised: May 28, 2026
Accepted: June 5, 2026
Published: July 9, 2026



ACS Publications
© 2026 The Authors. Published by American Chemical Society

https://doi.org/10.1021/acs.nanolett.6c01807
Nano Lett. 2026, 26, 9143−9150

Downloaded from http://pubs.acs.org/naletd/article-pdf/26/28/9143/6583010/7/acs.nanolett.6c01807.pdf by TU DELFT user on 06 August 2026

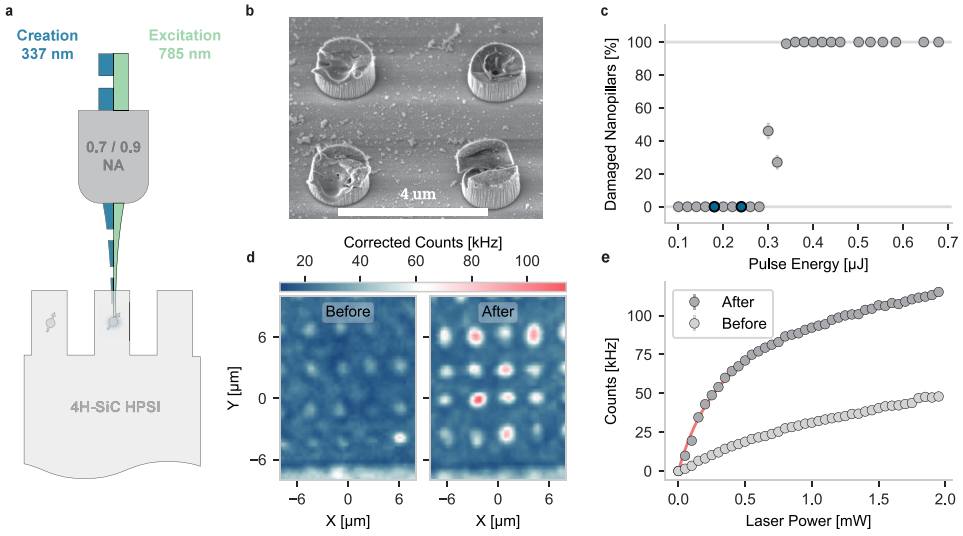


Figure 1. Laser-induced defect creation using an above-bandgap pulsed laser. a) Schematic of the laser-induced creation and detection of defects in HPSI 4H-SiC. A 0.7 NA objective focuses an above-bandgap (337 nm) pulsed (3 ns) laser onto the center of the nanopillar to create defects. For imaging, we use a 0.9 NA objective and a 785 nm laser for off-resonant excitation. **b)** Scanning electron microscopy image of the HPSI amorphized nanopillars that were exposed to a single UV pulse with energies higher than the LIAT (0.28 μJ). The nanopillars are ∼1.2 μm in diameter and ∼4 μm spaced from center to center. **c)** Amorphization statistics of nanopillars using a single pulse. For each pulse energy, one hundred nanopillars were each illuminated with a single pulse, and the percentage of nanopillars that showed visible damage is indicated on the *y*-axis. Blue dots indicate 0.18 μJ and 0.24 μJ, which are used for Figure 2 and Figure 3. See Figure S1 for SEM pictures of amorphization. **d)** 2D PL scans before and after a single UV pulse of 0.24 μJ at each pillar. The counts for both measurements were corrected to have the same background counts in bulk close to the nanopillars (before counts ×1.524, and after counts ×0.656, see Supporting Note S5 for correction method). **e)** Fluorescence saturation measurements before and after a single UV pulse of 0.24 μJ on the same pillar.

same type of nanopillars. Finally, we demonstrate long electron-spin coherence times (up to 3.6(3) ms) for laser-induced V2 centers, similar to values reported in high-quality epitaxial 4H-SiC.[11,34] The demonstration of spatially selective defect creation after device fabrication, with good optical and spin coherence in nanostructures made of commercial bulk-grown wafers, indicates that above-bandgap pulsed-laser illumination is a promising route toward scalable generation of coherent V2 centers in 4H-SiC devices.

We use an above-bandgap (337 nm, 3.68 eV) pulsed (3 ns) laser (similar as Day et al.[30]) focused on the sample via a 0.7 NA objective and investigate single-pulse defect creation in c-plane HPSI 4H-SiC with a bandgap of 3.26 eV[35] (Figure 1a,b, see Supporting Note S1 for sample preparation and Supporting Note S16 for the optical setups). Given the high efficiency of electron−hole pair generation at above-bandgap excitation, the material is susceptible to irreversible damage under intense irradiation.[30] To mitigate this, we first determine the laser-induced amorphization threshold (LIAT)[36,37] for both nanopillars and bulk HPSI 4H-SiC. This is achieved by exposing one hundred discrete spots per pulse energy (see Supporting Note S2). After UV illumination, scanning electron microscopy (SEM) is used to quantify the number of sites exhibiting resolvable surface amorphization (Supporting Note S3). We note that our analysis is limited to SEM-detectable surface amorphization, which excludes subsurface lattice damage.

Despite being limited to surface-level observations, our analysis enables the identification of three distinct regimes: no visible amorphization, probabilistic amorphization, and deterministic amorphization, observed in both the nanopillars (Figure 1c) and bulk material (Supporting Note S3). We find that the LIAT for nanopillars (>0.28 μJ) is lower compared to bulk (>0.32 μJ), showing that it is dependent on the nanophotonic structure (consistent with previous studies[38]).

With the LIAT determined, we verify that defect creation is possible at energies below this threshold. We perform off-resonant (785 nm) 2D photoluminescence (PL) scans before and after a single UV laser pulse for pulse energies below the LIAT, employing a 0.9 NA objective to improve collection efficiency (Supporting Note S4). An example of one of these 2D PL scans can be found in Figure 1d. For pulse energies ≥0.18 μJ, the 2D PL scans show an increase in PL for nearly all nanopillars (see Supporting Note S5), indicating subsurface lattice deformation or laser-induced defect generation.[39] Next, we perform fluorescence saturation measurements under off-resonant laser excitation on each individual nanopillar. These measurements reveal early saturation effects, associated with quantum-defect emission, for UV pulse energies ≥0.18 μJ, see Supporting Note S6. This suggests that laser-induced defect creation occurs over a broad parameter space, providing a usable energy window (0.18 μJ to 0.28 μJ) in which color centers can be introduced without inducing amorphization.

To further characterize UV-pulse-induced defect creation, we perform fluorescence saturation measurements on an additional 64 nanopillars before and after a single 0.18 μJ UV pulse (low-probability regime), and on 64 nanopillars exposed to a 0.24 μJ pulse (higher-probability regime). An example of a nanopillar fluorescence saturation measurement before and after a single pulse can be seen in Figure 1e.

To determine whether the observed increase in PL arises from the presence of V2 centers, we search for the characteristic zero-phonon line emission, corresponding to the A1 and A2 optical transitions, through photoluminescence excitation spectroscopy (PLE) spectra at 4 K.[17,40] We then compare the occurrence of V2 center peaks after exposure with a single UV pulse (0.18 μJ or 0.24 μJ) relative to the natural

https://doi.org/10.1021/acs.nanolett.6c01807
Nano Lett. 2026, 26, 9143−9150

Downloaded from http://pubs.acs.org/nalefd/article-pdf/26/28/9143/6583107/acs.nanolett.6c01807.pdf by TU DELFT user on 06 August 2026

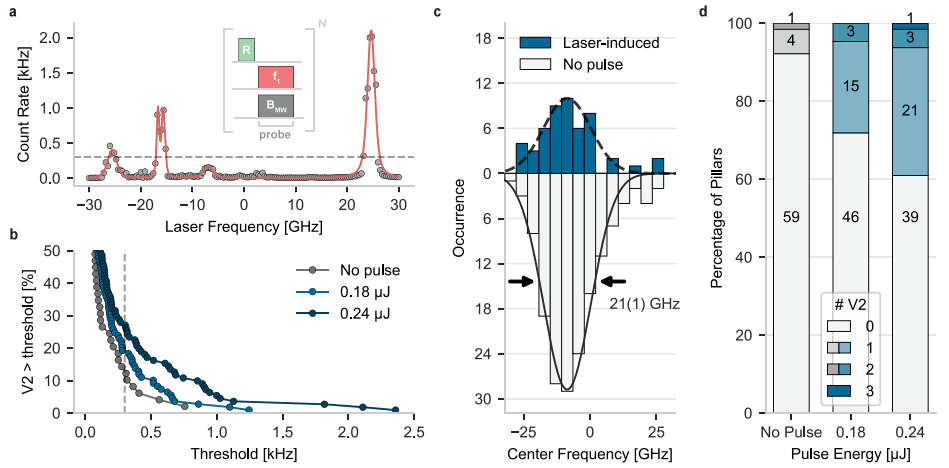


Figure 2. Photoluminescence excitation spectroscopy (PLE) and number of V2 centers. a) Single PLE of a nanopillar with three V2 centers passing a threshold (dashed gray line) at 0.3 kHz. Laser frequency is offset from 327.112 THz. Inset shows the experimental sequence, green indicates an off-resonant (repump) pulse (10 μs, 10 μW), and red indicates a single resonant laser (2 ms, 100 nW). Gray indicates microwaves (MW) at (70 MHz) to counteract spin pumping. **b)** Percentage of V2 centers whose fitted peak amplitude exceeds the count-rate threshold, shown separately for nanopillars exposed to a UV pulse (0.18 μJ and 0.24 μJ) and those left unexposed; in each condition, $n = 64$ nanopillars are examined. We find a maximum count rate for the nonexposed V2 center of 0.76 kHz. For this threshold, we also observe 3 and 11 times more V2 centers with the same or higher count rate at UV laser powers of 0.18 μJ and 0.24 μJ, respectively. **c)** Ensemble inhomogeneous distribution of all V2 centers in unexposed nanopillars (bottom gray bars). A Gaussian fit yields an fwhm of the inhomogeneous distribution of 22(1) GHz. The blue bars indicate the frequencies of the V2 centers in the UV-exposed nanopillars that pass the threshold of 0.3 kHz (this threshold sets a cutoff to suppress bulk-V2 contributions, also indicated by the dotted line in b)). The black dashed line shows the (scaled) Gaussian fit of the unexposed inhomogeneous distribution as a guide to the eye. **d)** Number of nanopillars that contain either 0, 1, 2, or 3 V2 centers that pass the 0.3 kHz threshold. Nanopillars exposed to the UV laser are shown in shades of blue, while natural (unexposed) V2 centers are shown in shades of gray. The numbers inside the bars show how many pillars contain that specific number of V2 centers.

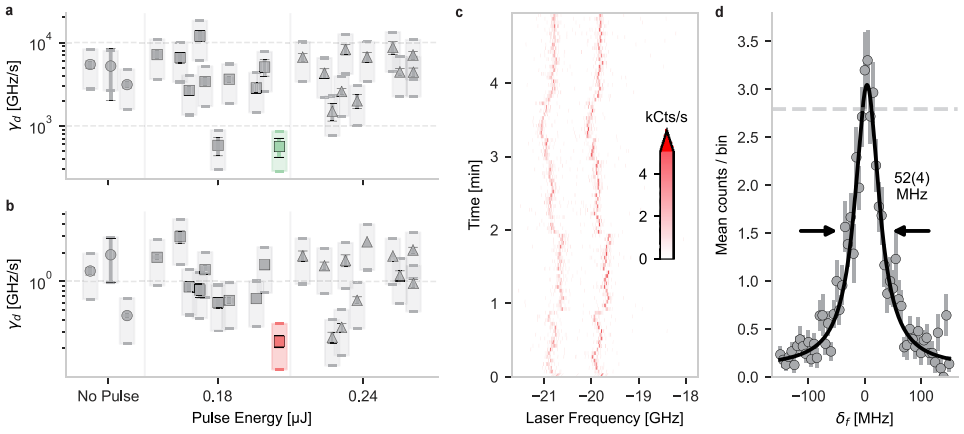


Figure 3. V2 optical properties and spectral diffusion. a) Fitted spectral diffusion constant under off-resonant excitation for natural V2 centers (circles) and laser-induced V2 centers (squares and triangles, 0.18 μJ and 0.24 μJ respectively). We extract γ_d using the methodology described in van de Stolpe et al.,[23] assuming a homogeneous line width (fwhm) of 36 MHz. Because the fitted γ_d depends on this homogeneous line width (see Supporting Note S10), and this line width was not measured for each individual V2 center, we indicate the spread in γ_d for a plausible range of line widths ($1 \leq \Gamma/\Gamma_{\text{lifetime}} \leq 3$, see Supporting Note S11). γ_d of the red square indicates the same V2 center as the green square in b) and data in c) and d). **b)** Fitted spectral diffusion constants under resonant excitation. **c)** Scanning laser PLE over 5 min of the V2 center highlighted in a) and b) (Pillar 14, Figure S7). The laser is on for a total of 334 ms per scan with a power at the objective of 20 nW. **d)** Check-probe PLE (see van de Stolpe et al.[23] and Supporting Note S11 for methodology) with fwhm = 52(4)MHz indicating similar optical line width ($\Gamma/\Gamma_{\text{lifetime}} = 2.21(4)$, see Figure S17) as natural V2 centers in this material (see Figure S16). Check-probe PLE was performed at a magnetic field of ~20 G aligned along the crystal *c*-axis (see Supporting Note S12).

occurrence (without UV pulse). We fit all PLE spectra (see Supporting Note S7, Supporting Note S8 and Supporting Note S9) and compare the frequencies and amplitudes of the fitted peaks (example of PLE in Figure 2a). Evaluating the percentage of V2 centers with peak amplitudes above a certain threshold reveals a significantly larger number of high-count-rate V2 centers in UV-exposed nanopillars (see Figure 2b). Relative to the brightest V2 center in the nonexposed nanopillars (0.76(2) kHz), nanopillars exposed to a 0.18 μJ or 0.24 μJ UV pulse contain roughly 3 and 11 times more V2 centers that reach or exceed this brightness, respectively. Furthermore, the brightest V2 center found in the UV-exposed nanopillars has a count rate of 2.11(4) kHz, approximately a factor of 2.8 higher than the brightest emitter in the nonexposed nanopillars.

https://doi.org/10.1021/acs.nanolett.6c01807
Nano Lett. 2026, 26, 9143−9150

Downloaded from http://pubs.acs.org/nalefd/article-pdf/26/28/9143/6583010/7/acs.nanolett.6c01807.pdf by TU DELFT user on 06 August 2026

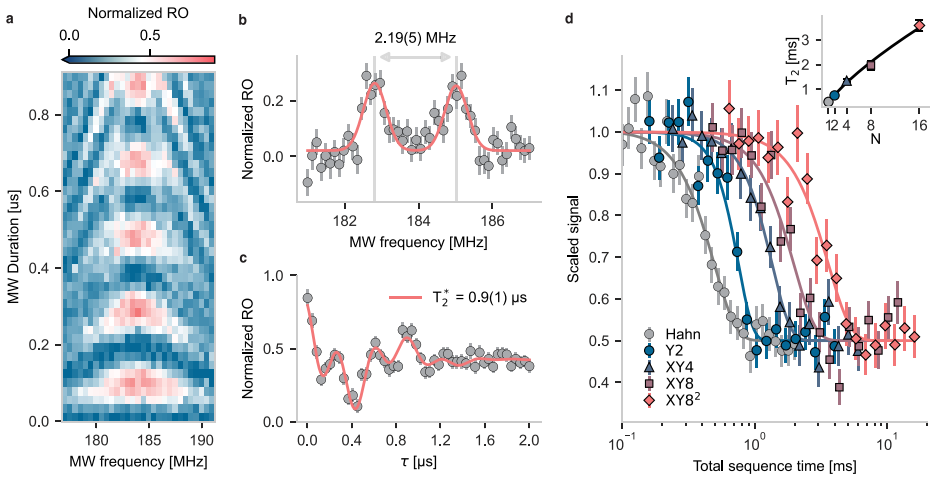


Figure 4. Electron spin properties. a) Rabi chevron pattern from the V2 center in pillar 9. Details on the measurement sequence and normalization procedure are elaborated in Supporting Note S14. **b)** Electron-spin-resonance of the same V2 center revealing a strongly coupled nuclear spin with hyperfine splitting of 2.19(5) MHz (red line). **c)** Detuned Ramsey measurement on the same V2 center with f_{MW} = 181.8 MHz. Red line indicates a fit to an oscillation with two frequency components and a Gaussian decay, which translates to a hyperfine splitting of f_{HF} = 2.08(7)MHz, consistent with the measurement in b), and $T_2^* = 0.9(1)$ μs. **d)** Scaled Hahn-echo ($N = 1$) and dynamical decoupling ($N = 2$ to $N = 16$) measurements on the V2 center in pillar 14 (Figure S7) with no (resolvable) strongly coupled nuclear spin (see Figure S23 for Chevron, ESR and Ramsey) at a magnetic field of ∼1300 G. We find a $T_2^{Hahn} = 0.49(2)$ ms and extend the coherence time to $T_2^{DD} = 3.6(3)$ ms with two XY8 sequences. The inset shows T_2 as a function of the number of π-pulses N, fitted to a power function $T_2 = \beta \cdot N^{\alpha}$ (excluding Hahn-echo) from which we extract $\alpha = 0.73(4)$ and $\beta = 0.46(4)$ ms.

Because weak background emission can originate from defects outside the nanopillars, we restrict our analysis to V2 centers with a PLE amplitude above 0.3 kHz (dotted line, Figure 2a,b). This threshold ensures that only bright, well-collected V2 centers (most likely located near the nanopillar center, see Supporting Note S4) are included.

Using the 0.3 kHz threshold, we find that the frequencies of the V2 centers in the UV-exposed nanopillars follow the same ensemble inhomogeneous distribution as the natural V2 center population (Figure 2c). This suggests that the UV pulse does not introduce significant strain or amorphization in the vicinity of the laser-induced V2 centers.[22,41,42] Furthermore, we quantify the probability of inducing only one bright V2 center for the two UV pulse energies (Figure 2d). After a single 0.18 μJ pulse, ∼23% of the nanopillars contain one bright V2 center, increasing to ∼33% for 0.24 μJ. For comparison, this is observed in only ∼6% of nonexposed nanopillars. These results show that the UV-pulse strongly increases the number of V2 centers, even though the exact origin of each V2 center, whether created by the UV-pulse or naturally present, cannot be determined unambiguously. As we will show below, the optical properties of V2 centers with and without UV illumination are very similar, so this ambiguity does not affect the conclusion that the UV pulse induces high-quality V2 centers. In the remainder of this work, we will therefore refer to V2 centers in UV-exposed nanopillars as laser-induced V2 centers and in nonexposed nanopillars as natural V2 centers.

Next, we characterize the optical properties of the laser-induced V2 centers and compare them to natural V2 centers using the check-probe spectroscopy methodology of van de Stolpe et al.[23] We characterized 24 individual V2 centers, including 3 natural (circles in Figure 3a,b) and 21 laser-induced centers. Among the laser-induced centers, 10 were exposed to a single UV pulse with an energy of 0.18 μJ (squares), while 11 were exposed to a single pulse with an energy of 0.24 μJ (triangles).

The measured spectral diffusion rates under resonant and off-resonant excitation are shown in Figure 3a,b. This reveals a 3−4 orders-of-magnitude difference in spectral diffusion between resonant and off-resonant laser light, consistent with previous work.[23] Additionally, we observe a significant spread in spectral diffusion rates, indicating that each V2 center experiences a distinct local charge environment. Importantly, we find no significant difference in the spectral diffusion rates between laser-induced and natural V2 centers; the two groups exhibit similar overall distributions. This suggests that the single UV pulse does not substantially alter the effective local charge environment, and that the impurities of the HPSI material or the embedding in a nanopillar, are still the main cause of spectral diffusion.[42] Within the distribution of spectral diffusion constants (γ_d) for laser-induced V2 centers, some V2 centers remain particularly stable, exhibiting low γ_d even under off-resonant excitation (green and red markers in Figure 3a,b).

We perform two additional types of photoluminescence excitation (PLE) measurements. First, we observe the spectral wandering (Figure 3c) by scanning a resonant laser continuously while applying microwaves; second, we use a check-probe type PLE on the A1 transition to approximate the homogeneous line width (Figure 3d).[23] By sweeping the threshold for the check-probe PLE, we can minimize the residual broadening due to imperfect initialization and compare this homogeneous line width to the lifetime-limited line width (see Supporting Note S11). We find line widths satisfying $1 \leq \Gamma/\Gamma_{lifetime} \leq 4$ for all measured V2 centers, indicating that there is still some broadening (either residual (in)homogeneous broadening, or power broadening). The line widths for the natural V2 centers are similar to the laser-induced V2 centers, indicating that the UV pulse does not significantly lower the optical coherence of the V2 centers and, importantly, are compatible with remote entanglement generation under modest time filtering.[43]

https://doi.org/10.1021/acs.nanolett.6c01807
Nano Lett. 2026, 26, 9143−9150

Downloaded from http://pubs.acs.org/naletd/article-pdf/26/28/9143/6583010/7/acs.nanolett.6c01807.pdf by TU DELFT user on 06 August 2026

In addition to optical coherence, the electron spin coherence is a crucial component for utilizing laser-induced V2 centers in sensing, quantum information processing, and quantum network applications. We investigate the spin properties of two single laser-induced V2 centers, which exhibits relatively low spectral diffusion (γ_d) under both resonant and off-resonant excitation (pillar 9 and 14; see Figure S7 for location details, Supporting Note S13 for optical properties of V2 center in pillar 9, Figure 3c,d for optical properties of V2 center in pillar 14 and Figure S23 for spin properties of V2 center in pillar 14). Note that this optical selection might already introduce a bias in the electron spin environment and thus, potentially in the electron spin coherence.

First, we operate at a magnetic field of ∼40 G. This ensures that the Kramers degeneracy within the $\pm\frac{1}{2}$ and $\pm\frac{3}{2}$ spin eigenstates is lifted, and that the ground or excited state level crossings are sufficiently detuned.[42,44,45] Figure 4a shows Rabi oscillations for driving the ground state $\left|m_s = +\frac{1}{2}\right\rangle \leftrightarrow \left|m_s = +\frac{3}{2}\right\rangle$ transition of the V2 center found in pillar 9. On the same V2 center, we perform electron spin resonance (ESR), see Figure 4b (details of the sequence can be found in Supporting Note S14). ESR reveals a strongly coupled nuclear spin, with a hyperfine coupling of 2.19(5) MHz. This coupling is consistent with either a coupled ^{13}C or ^{29}Si nuclear spin as previously observed and reported,[46] and accounts for the detuning visible in the Rabi chevron pattern (Figure 4a and Supporting Note S14). We perform Ramsey measurements to extract the spin-dephasing time T_2^*, finding $T_2^* = 0.9(1)\ \mu s$ (Figure 4c).

Next, we operate at a higher magnetic field (∼1300 G) to suppress decoherence from anisotropic hyperfine interactions with the spin bath. We perform Hahn-echo and dynamical decoupling (DD) measurements on the V2 center in pillar 14, which has no strongly coupled nuclear spins. We measure a Hahn-echo coherence time of $T_2^{Hahn} = 0.49(2)$ ms and extend the coherence up to $T_2^{DD} = 3.6(3)$ ms using two consecutive XY8 sequences (Figure 4d).

The T_2^{DD} values display a power-law dependence on the number of decoupling pulses, with a fitted exponent of $\alpha = 0.73(4)$. This is slightly higher than the $\alpha = 2/3$ scaling associated with a Lorentzian noise spectrum $\left(\sim\frac{1}{\omega^2}\right)$, characteristic of Ornstein−Uhlenbeck dynamics,[47] indicating a slight deviation from a single-Lorentzian noise spectrum toward lower frequency noise.[48] Despite the relatively high nitrogen concentration of ($\sim 1.1 \times 10^{15}\ cm^{-3}$, see Supporting Note S1) our T_2^* and T_2^{Hahn} are comparable to values reported for natural-isotope-abundance epitaxially grown 4H-SiC with doping levels 2 orders of magnitude lower.[11,34,49−52] This suggests that neither the doping level nor the laser-writing method limits the spin coherence. These results show that commercially available wafers combined with laser-induced defect creation might provide a viable path toward quantum technologies based on color centers in 4H-SiC.

In this work, we studied the creation of laser-induced V2 centers in 4H-SiC nanopillars in bulk-grown SiC. We observe narrow optical line widths that are compatible with remote entanglement generation,[43] and long electron-spin coherence times consistent with dephasing by the nuclear spin bath,[11] although potential contributions from electron spin impurities cannot be excluded.

Looking forward, while here we focus on the formation of V2 centers in bulk-grown 4H-SiC wafers, the methods employed here can potentially be extended to high-quality, isotopically engineered, epitaxially grown 4H-SiC,[53−57] and as well to other defect centers, such as V1 centers (h-site V_{Si}^-),[40] divacancies,[14] and non-native atom-related complexes like NV centers.[15] A systematic exploration of defect formation, density, and properties using above-bandgap laser writing, across different irradiation conditions and writing parameters, can enable deeper insight into the underlying material science and the mechanisms of defect creation, including potential local annealing or activation effects,[58] in different types of SiC and nanostructures.

Additionally, monitoring the photoluminescence between laser pulses might enable the deterministic creation of a desired number of defects.[29] Large-scale fabrication methods, such as Silicon-Carbide-on-Insulator[5] or angled etching,[10] would open the door to complex integrated nanophotonic structures, including photonic crystal cavities. Together with the laser-induced creation of high-quality V2 centers in commercial bulk-grown SiC wafers presented here, this combination might enable a path toward efficient, high-quality defect creation in scalable quantum devices.

■ ASSOCIATED CONTENT

Data Availability Statement

All data underlying the study are available on the open 4TU data server: 10.4121/be9e8523-5fb9-4861-abad-95b71231c086. Code used to operate the experiments is available on request.

Supporting Information

The Supporting Information is available free of charge at https://pubs.acs.org/doi/10.1021/acs.nanolett.6c01807.

Sample preparation; pulsed UV experiments; examples of SEM images used to determine the laser-induced amorphization threshold; simulated comparison of collection efficiency with different NA objectives; additional data on room-temperature photoluminescence and laser saturation measurements; PLE V2 selection; locations of the observed V2 centers together with the photoluminescence excitation measurements; Hanbury Brown Twiss experiments for several V2 centers; methods for characterizing the spectral diffusion rate and homogeneous line widths, together with data of several V2 centers; magnetic field alignment; pulse scheme and simulations of the spin measurements; spin coherence at low magnetic field; schematics of optical setups (PDF)

■ AUTHOR INFORMATION

Corresponding Author

Tim H. Taminiau − *QuTech and Kavli Institute of Nanoscience Delft, Delft University of Technology, 2600 GA Delft, The Netherlands*; Email: t.h.taminiau@tudelft.nl

Authors

Laurens J. Feije − *QuTech and Kavli Institute of Nanoscience Delft, Delft University of Technology, 2600 GA Delft, The Netherlands*; orcid.org/0009-0009-6909-9145

https://doi.org/10.1021/acs.nanolett.6c01807
Nano Lett. 2026, 26, 9143−9150

Downloaded from http://pubs.acs.org/naletf/article-pdf/26/28/9143/6583010/7/acs.nanolett.6c01807.pdf by TU DELFT user on 06 August 2026

Gerben M. Timmer − *QuTech and Kavli Institute of Nanoscience Delft, Delft University of Technology, 2600 GA Delft, The Netherlands*
Yihong Hu − *QuTech and Kavli Institute of Nanoscience Delft, Delft University of Technology, 2600 GA Delft, The Netherlands;* orcid.org/0009-0006-4525-9456
Rana Karababa − *QuTech and Kavli Institute of Nanoscience Delft, Delft University of Technology, 2600 GA Delft, The Netherlands*
Guido L. van de Stolpe − *QuTech and Kavli Institute of Nanoscience Delft, Delft University of Technology, 2600 GA Delft, The Netherlands*
Tobias Martens − *QuTech and Kavli Institute of Nanoscience Delft, Delft University of Technology, 2600 GA Delft, The Netherlands;* orcid.org/0009-0008-9800-7548
Sjoerd J. H. Loenen − *QuTech and Kavli Institute of Nanoscience Delft, Delft University of Technology, 2600 GA Delft, The Netherlands;* orcid.org/0000-0001-9154-6794
Theo B. A. Durant − *QuTech and Kavli Institute of Nanoscience Delft, Delft University of Technology, 2600 GA Delft, The Netherlands*
Antariksha Das − *QuTech and Kavli Institute of Nanoscience Delft, Delft University of Technology, 2600 GA Delft, The Netherlands;* orcid.org/0000-0002-4248-087X
Aaron M. Day − *John A. Paulson School of Engineering and Applied Sciences, Harvard University, Cambridge, Massachusetts 02138, United States;* orcid.org/0000-0003-2973-9434
Evelyn L. Hu − *John A. Paulson School of Engineering and Applied Sciences, Harvard University, Cambridge, Massachusetts 02138, United States*

Complete contact information is available at: https://pubs.acs.org/10.1021/acs.nanolett.6c01807

Author Contributions

[‖]LJF and GMT contributed equally. LJF, GMT, and RK performed the room temperature creation and detection experiments with analytical and discussion support from AMD and ELH. GMT and RK performed the amorphization threshold measurements. GMT designed and fabricated the sample. LJF, YH, and TM performed the low-temperature optical and spin property measurements. GvdS, SJHL, LJF, GMT, RK, TD, and AD built the experimental apparatus. LJF, GMT, RK, YH ,and THT analyzed the data. LJF, GMT, YH, and THT wrote the manuscript with input from all authors. THT supervised the project.

Notes

The authors declare no competing financial interest.

■ ACKNOWLEDGMENTS

We thank J. Dietz for the useful discussions on above-bandgap laser writing. We thank V. Vorobyov and F. Kaiser for the input on the optical setup and general discussions. We thank B. van Ommen, J. Yun, M. van Riggelen, and N. Demetriou for discussions on spin dynamics and control. We thank H. Beukers and C. Waas for their help with automating measurements. We thank N. Albert and T. Hiep for designing and machining parts for the setup, H. Ervasti, P. Botma, and R. Budhrani for software support and development, R. Méjard and H. M. Amin for optical and safety support, S. Visser, V. Narain, and E. van der Wiel for general technical support, and J. Mensigh, O. Benningshof, and J. Croese for cryogenic and vacuum engineering support. This project has received funding from the European Research Council (ERC) under the European Union's Horizon 2020 research and innovation programme (grant agreement No. 852410). This work was supported by the Dutch National Growth Fund (NGF), as part of the Quantum Delta NL programme. This work is part of the research programme NWA-ORC with project number NWA.1160.18.208, which is (partly) financed by the Dutch Research Council (NWO). This project has received funding from the European Union's Horizon Europe research and innovation program under grant agreement No 101135699. This work was funded by the European Union's Horizon Europe research and innovation programme under grant agreement No. 101102140 − QIA Phase 1. This project was funded within the QuantERA II Programme that has received funding from the EU H2020 research and innovation programme under GA No 101017733.

■ REFERENCES

(1) Bradley, C. E.; Randall, J.; Abobeih, M. H.; Berrevoets, R. C.; Degen, M. J.; Bakker, M. A.; Markham, M.; Twitchen, D. J.; Taminiau, T. H. A Ten-Qubit Solid-State Spin Register with Quantum Memory up to One Minute. *Physical Review X* **2019**, *9*, 031045.
(2) Stolk, A. J.; et al. Metropolitan-Scale Heralded Entanglement of Solid-State Qubits. *Science Advances* **2024**, *10*, No. eadp6442.
(3) Pompili, M.; Hermans, S. L. N.; Baier, S.; Beukers, H. K. C.; Humphreys, P. C.; Schouten, R. N.; Vermeulen, R. F. L.; Tiggelman, M. J.; dos Santos Martins, L.; Dirkse, B.; Wehner, S.; Hanson, R. Realization of a Multinode Quantum Network of Remote Solid-State Qubits. *Science* **2021**, *372*, 259−264.
(4) Knaut, C. M.; et al. Entanglement of Nanophotonic Quantum Memory Nodes in a Telecom Network. *Nature* **2024**, *629*, 573−578.
(5) Lukin, D. M.; Dory, C.; Guidry, M. A.; Yang, K. Y.; Mishra, S. D.; Trivedi, R.; Radulaski, M.; Sun, S.; Vercruysse, D.; Ahn, G. H.; Vučković, J. 4H-silicon-carbide-on-insulator for Integrated Quantum and Nonlinear Photonics. *Nat. Photonics* **2020**, *14*, 330−334.
(6) Harris, I. B. W. et al. High-Fidelity Control of a Strongly Coupled Electro-Nuclear Spin-Photon Interface. *arXiv* 2025, arXiv:2505.09267.
(7) Ruf, M.; IJspeert, M.; van Dam, S.; de Jong, N.; van den Berg, H.; Evers, G.; Hanson, R. Optically Coherent Nitrogen-Vacancy Centers in Micrometer-Thin Etched Diamond Membranes. *Nano Lett.* **2019**, *19*, 3987−3992.
(8) van Dam, S. B.; Walsh, M.; Degen, M. J.; Bersin, E.; Mouradian, S. L.; Galiullin, A.; Ruf, M.; IJspeert, M.; Taminiau, T. H.; Hanson, R.; Englund, D. R. Optical Coherence of Diamond Nitrogen-Vacancy Centers Formed by Ion Implantation and Annealing. *Phys. Rev. B* **2019**, *99*, 161203.
(9) González-Tudela, A.; Reiserer, A.; García-Ripoll, J. J.; García-Vidal, F. J. Light−Matter Interactions in Quantum Nanophotonic Devices. *Nature Reviews Physics* **2024**, *6*, 166−179.
(10) Majety, S.; Norman, V. A.; Saha, P.; Rubin, A. H.; Dhuey, S.; Radulaski, M. Wafer-Scale Integration of Freestanding Photonic Devices with Color Centers in Silicon Carbide. *npj Nanophotonics* **2025**, *2*, 3.
(11) Steidl, T.; Kuna, P.; Hesselmeier-Hüttmann, E.; Liu, D.; Stöhr, R.; Knolle, W.; Ghezellou, M.; Ul-Hassan, J.; Schober, M.; Bockstedte, M.; Bian, G.; Gali, A.; Vorobyov, V.; Wrachtrup, J. Single V2 Defect in 4H Silicon Carbide Schottky Diode at Low Temperature. *Nat. Commun.* **2025**, *16*, 4669.
(12) Christle, D. J.; Falk, A. L.; Andrich, P.; Klimov, P. V.; Hassan, J. U.; Son, N. T.; Janzén, E.; Ohshima, T.; Awschalom, D. D. Isolated Electron Spins in Silicon Carbide with Millisecond Coherence Times. *Nat. Mater.* **2015**, *14*, 160−163.
(13) Son, N. T.; Anderson, C. P.; Bourassa, A.; Miao, K. C.; Babin, C.; Widmann, M.; Niethammer, M.; Ul Hassan, J.; Morioka, N.;

Downloaded from http://pubs.acs.org/naletd/article-pdf/26/28/9143/6583010/7/acs.nanolett.6c01807.pdf by TU DELFT user on 06 August 2026

Ivanov, I. G.; Kaiser, F.; Wrachtrup, J.; Awschalom, D. D. Developing Silicon Carbide for Quantum Spintronics. *Appl. Phys. Lett.* **2020**, *116*, 190501.
(14) Anderson, C. P.; Glen, E. O.; Zeledon, C.; Bourassa, A.; Jin, Y.; Zhu, Y.; Vorwerk, C.; Crook, A. L.; Abe, H.; Ul-Hassan, J.; Ohshima, T.; Son, N. T.; Galli, G.; Awschalom, D. D. Five-Second Coherence of a Single Spin with Single-Shot Readout in Silicon Carbide. *Science Advances* **2022**, *8*, No. eabm5912.
(15) Norman, V. A.; Majety, S.; Rubin, A. H.; Saha, P.; Gonzalez, N. R.; Simo, J.; Palomarez, B.; Li, L.; Curro, P. B.; Dhuey, S.; Virasawmy, S.; Radulaski, M. Sub-2 K Characterization of Nitrogen-Vacancy Centers in Silicon Carbide Nanopillars. *ACS Photonics* **2025**, *12*, 2604−2611.
(16) Hessenauer, J.; Körber, J.; Ghezellou, M.; Ul-Hassan, J.; Astakhov, G. V.; Knolle, W.; Wrachtrup, J.; Hunger, D. Cavity Enhancement of V2 Centers in 4H-SiC with a Fiber-Based Fabry−Perot Microcavity. *Optica Quantum* **2025**, *3*, 175−181.
(17) Liu, D.; Kaiser, F.; Bushmakin, V.; Hesselmeier, E.; Steidl, T.; Ohshima, T.; Son, N. T.; Ul-Hassan, J.; Soykal, Ö. O.; Wrachtrup, J. The Silicon Vacancy Centers in SiC: Determination of Intrinsic Spin Dynamics for Integrated Quantum Photonics. *npj Quantum Information* **2024**, *10*, 72.
(18) Astner, T.; Koller, P.; Gilardoni, C. M.; Hendriks, J.; Tien Son, N.; Ivanov, I. G.; Ul Hassan, J.; van der Wal, C. H.; Trupke, M. Vanadium in Silicon Carbide: Telecom-Ready Spin Centres with Long Relaxation Lifetimes and Hyperfine-Resolved Optical Transitions. *Quantum Science and Technology* **2024**, *9*, 035038.
(19) Wolfowicz, G.; Anderson, C. P.; Diler, B.; Poluektov, O. G.; Heremans, F. J.; Awschalom, D. D. Vanadium Spin Qubits as Telecom Quantum Emitters in Silicon Carbide. *Science Advances* **2020**, *6*, No. eaaz1192.
(20) Cilibrizzi, P.; Arshad, M. J.; Tissot, B.; Son, N. T.; Ivanov, I. G.; Astner, T.; Koller, P.; Ghezellou, M.; Ul-Hassan, J.; White, D.; Bekker, C.; Burkard, G.; Trupke, M.; Bonato, C. Ultra-Narrow Inhomogeneous Spectral Distribution of Telecom-Wavelength Vanadium Centres in Isotopically-Enriched Silicon Carbide. *Nat. Commun.* **2023**, *14*, 8448.
(21) Babin, C.; et al. Fabrication and Nanophotonic Waveguide Integration of Silicon Carbide Colour Centres with Preserved Spin-Optical Coherence. *Nat. Mater.* **2022**, *21*, 67−73.
(22) Heiler, J.; Körber, J.; Hesselmeier, E.; Kuna, P.; Stöhr, R.; Fuchs, P.; Ghezellou, M.; Ul-Hassan, J.; Knolle, W.; Becher, C.; Kaiser, F.; Wrachtrup, J. Spectral Stability of V2 Centres in Sub-Micron 4H-SiC Membranes. *npj Quantum Materials* **2024**, *9*, 34.
(23) van de Stolpe, G. L.; Feije, L. J.; Loenen, S. J. H.; Das, A.; Timmer, G. M.; de Jong, T. W.; Taminiau, T. H. Check-Probe Spectroscopy of Lifetime-Limited Emitters in Bulk-Grown Silicon Carbide. *npj Quantum Information* **2025**, *11*, 31.
(24) Wang, J.-F.; Li, Q.; Yan, F.-F.; Liu, H.; Guo, G.-P.; Zhang, W.-P.; Zhou, X.; Guo, L.-P.; Lin, Z.-H.; Cui, J.-M.; Xu, X.-Y.; Xu, J.-S.; Li, C.-F.; Guo, G.-C. On-Demand Generation of Single Silicon Vacancy Defects in Silicon Carbide. *ACS Photonics* **2019**, *6*, 1736−1743.
(25) Pavunny, S. P.; Yeats, A. L.; Banks, H. B.; Bielejec, E.; Myers-Ward, R. L.; DeJarld, M. T.; Bracker, A. S.; Gaskill, D. K.; Carter, S. G. Arrays of Si Vacancies in 4H-SiC Produced by Focused Li Ion Beam Implantation. *Sci. Rep.* **2021**, *11*, 3561.
(26) He, Z.-X.; Li, Q.; Wen, X.-L.; Zhou, J.-Y.; Lin, W.-X.; Hao, Z.-H.; Xu, J.-S.; Li, C.-F.; Guo, G.-C. Maskless Generation of Single Silicon Vacancy Arrays in Silicon Carbide by a Focused He+ Ion Beam. *ACS Photonics* **2023**, *10*, 2234−2240.
(27) Wang, J.; Zhang, X.; Zhou, Y.; Li, K.; Wang, Z.; Peddibhotla, P.; Liu, F.; Bauerdick, S.; Rudzinski, A.; Liu, Z.; Gao, W. Scalable Fabrication of Single Silicon Vacancy Defect Arrays in Silicon Carbide Using Focused Ion Beam. *ACS Photonics* **2017**, *4*, 1054−1059.
(28) Chandrasekaran, V.; Titze, M.; Flores, A. R.; Campbell, D.; Henshaw, J.; Jones, A. C.; Bielejec, E. S.; Htoon, H. High-Yield Deterministic Focused Ion Beam Implantation of Quantum Defects Enabled by In Situ Photoluminescence Feedback. *Advanced Science* **2023**, *10*, 2300190.
(29) Chen, Y.-C.; Griffiths, B.; Weng, L.; Nicley, S. S.; Ishmael, S. N.; Lekhai, Y.; Johnson, S.; Stephen, C. J.; Green, B. L.; Morley, G. W.; Newton, M. E.; Booth, M. J.; Salter, P. S.; Smith, J. M. Laser Writing of Individual Nitrogen-Vacancy Defects in Diamond with near-Unity Yield. *Optica* **2019**, *6*, 662−667.
(30) Day, A. M.; Dietz, J. R.; Sutula, M.; Yeh, M.; Hu, E. L. Laser Writing of Spin Defects in Nanophotonic Cavities. *Nat. Mater.* **2023**, *22*, 696−702.
(31) Hao, Z.-H.; He, Z.-X.; Maksimovic, J.; Katkus, T.; Xu, J.-S.; Juodkazis, S.; Li, C.-F.; Guo, G.-C.; Castelletto, S. Laser Writing and Spin Control of Near-Infrared Emitters in Silicon Carbide. *ACS Photonics* **2025**, *12*, 1552−1560.
(32) Jones, A. R.; Cheng, X.; Parthasarathy, S. K.; Arshad, M. J.; Cilibrizzi, P.; Nagy, R.; Salter, P.; Smith, J.; Bonato, C.; Bekker, C. Scalable Registration of Single Quantum Emitters within Solid Immersion Lenses through Femtosecond Laser Writing. *Nano Lett.* **2025**, *25*, 11528−11535.
(33) Chen, Y.-C.; Salter, P. S.; Niethammer, M.; Widmann, M.; Kaiser, F.; Nagy, R.; Morioka, N.; Babin, C.; Erlekampf, J.; Berwian, P.; Booth, M. J.; Wrachtrup, J. Laser Writing of Scalable Single Color Centers in Silicon Carbide. *Nano Lett.* **2019**, *19*, 2377−2383.
(34) Kuna, P.; Hesselmeier-Hüttmann, E.; Schillinger, P.; Gloistein, F.; Takács, I.; Ivády, V.; Knolle, W.; Ul-Hassan, J.; Wrachtrup, J.; Vorobyov, V. Localization and Coherent Control of 25 Nuclear Spins in Silicon Carbide. *arXiv* 2025, arXiv:2512.20281.
(35) Son, N. T.; Ivanov, I. G. Charge State Control of the Silicon Vacancy and Divacancy in Silicon Carbide. *J. Appl. Phys.* **2021**, *129*, 215702.
(36) Wood, R. M. *Laser-Induced Damage of Optical Materials*; CRC Press: Boca Raton, 2003.
(37) Nasiri, Z.; Fallah, H.; Hajimahmoodzadeh, M.; Mardiha, M. Investigation of the Laser-Induced Damage Thresholds of All-Dielectric and Metal-Dielectric Mirrors for a Continuous Wave at 10.6 μm. *Opt. Mater.* **2021**, *114*, 110936.
(38) Oliveira, B.; Claveria, P. S. M.; Araujo, P. D. R.; Estrela, P.; Gonçalves, I.; Nunes, M. I. S.; Meirinho, R.; Fajardo, M.; Piccardo, M. High-Aspect-Ratio, Ultratall Silica Meta-Optics for High-Intensity Structured Light. *Optica* **2025**, *12*, 713−719.
(39) Liu, X.; et al. Color Centers and Crystal Structural Transformations Induced by Femtosecond Laser Writing in 4H-SiC. *J. Appl. Phys.* **2025**, *137*, 123101.
(40) Nagy, R.; et al. High-Fidelity Spin and Optical Control of Single Silicon-Vacancy Centres in Silicon Carbide. *Nat. Commun.* **2019**, *10*, 1954.
(41) Körber, J.; Heiler, J.; Fuchs, P.; Flad, P.; Hesselmeier, E.; Kuna, P.; Ul-Hassan, J.; Knolle, W.; Becher, C.; Kaiser, F.; Wrachtrup, J. Fluorescence Enhancement of Single V2 Centers in a 4H-SiC Cavity Antenna. *Nano Lett.* **2024**, *24*, 9289−9295.
(42) Udvarhelyi, P.; Thiering, G.; Morioka, N.; Babin, C.; Kaiser, F.; Lukin, D.; Ohshima, T.; Ul-Hassan, J.; Son, N. T.; Vučković, J.; Wrachtrup, J.; Gali, A. Vibronic States and Their Effect on the Temperature and Strain Dependence of Silicon-Vacancy Qubits in 4H-SiC. *Physical Review Applied* **2020**, *13*, 054017.
(43) Legero, T.; Wilk, T.; Kuhn, A.; Rempe, G. Time-Resolved Two-Photon Quantum Interference. *Appl. Phys. B: Laser Opt.* **2003**, *77*, 797−802.
(44) Soykal, Ö. O.; Dev, P.; Economou, S. E. Silicon Vacancy Center in 4H-SiC: Electronic Structure and Spin-Photon Interfaces. *Phys. Rev. B* **2016**, *93*, 081207.
(45) Simin, D.; Soltamov, V. A.; Poshakinskiy, A. V.; Anisimov, A. N.; Babunts, R. A.; Tolmachev, D. O.; Mokhov, E. N.; Trupke, M.; Tarasenko, S. A.; Sperlich, A.; Baranov, P. G.; Dyakonov, V.; Astakhov, G. V. All-Optical Dc Nanotesla Magnetometry Using Silicon Vacancy Fine Structure in Isotopically Purified Silicon Carbide. *Physical Review X* **2016**, *6*, 031014.
(46) Hesselmeier, E.; Kuna, P.; Takács, I.; Ivády, V.; Knolle, W.; Son, N. T.; Ghezellou, M.; Ul-Hassan, J.; Dasari, D.; Kaiser, F.; Vorobyov, V.; Wrachtrup, J. Qudit-Based Spectroscopy for Measure-

Downloaded from http://pubs.acs.org/naletd/article-pdf/26/28/9143/6583010/7/acs.nanolett.6c01807.pdf by TU DELFT user on 06 August 2026

https://doi.org/10.1021/acs.nanolett.6c01807
Nano Lett. 2026, 26, 9143−9150

ment and Control of Nuclear-Spin Qubits in Silicon Carbide. *Phys. Rev. Lett.* **2024**, *132*, 090601.
(47) de Lange, G.; Wang, Z. H.; Ristè, D.; Dobrovitski, V. V.; Hanson, R. Universal Dynamical Decoupling of a Single Solid-State Spin from a Spin Bath. *Science* **2010**, *330*, 60−63.
(48) Medford, J.; Cywiński, Ł.; Barthel, C.; Marcus, C. M.; Hanson, M. P.; Gossard, A. C. Scaling of Dynamical Decoupling for Spin Qubits. *Phys. Rev. Lett.* **2012**, *108*, 086802.
(49) Lai, X.-Y.; Fang, R.-Z.; Li, T.; Su, R.-Z.; Huang, J.; Li, H.; You, L.-X.; Bao, X.-H.; Pan, J.-W. Single-Shot Readout of a Nuclear Spin in Silicon Carbide. *Phys. Rev. Lett.* **2024**, *132*, 180803.
(50) Nagy, R.; Widmann, M.; Niethammer, M.; Dasari, D. B. R.; Gerhardt, I.; Soykal, Ö. O.; Radulaski, M.; Ohshima, T.; Vučković, J.; Son, N. T.; Ivanov, I. G.; Economou, S. E.; Bonato, C.; Lee, S.-Y.; Wrachtrup, J. Quantum Properties of Dichroic Silicon Vacancies in Silicon Carbide. *Physical Review Applied* **2018**, *9*, 034022.
(51) Simin, D.; Kraus, H.; Sperlich, A.; Ohshima, T.; Astakhov, G. V.; Dyakonov, V. Locking of Electron Spin Coherence above 20 Ms in Natural Silicon Carbide. *Phys. Rev. B* **2017**, *95*, 161201.
(52) Yang, L.-P.; Burk, C.; Widmann, M.; Lee, S.-Y.; Wrachtrup, J.; Zhao, N. Electron Spin Decoherence in Silicon Carbide Nuclear Spin Bath. *Phys. Rev. B* **2014**, *90*, 241203.
(53) Bourassa, A.; Anderson, C. P.; Miao, K. C.; Onizhuk, M.; Ma, H.; Crook, A. L.; Abe, H.; Ul-Hassan, J.; Ohshima, T.; Son, N. T.; Galli, G.; Awschalom, D. D. Entanglement and Control of Single Nuclear Spins in Isotopically Engineered Silicon Carbide. *Nat. Mater.* **2020**, *19*, 1319−1325.
(54) Bulancea-Lindvall, O.; Eiles, M. T.; Son, N. T.; Abrikosov, I. A.; Ivády, V. Isotope-Purification-Induced Reduction of Spin-Relaxation and Spin-Coherence Times in Semiconductors. *Physical Review Applied* **2023**, *19*, 064046.
(55) Parthasarathy, S. K.; Kallinger, B.; Kaiser, F.; Berwian, P.; Dasari, D. B.; Friedrich, J.; Nagy, R. Scalable Quantum Memory Nodes Using Nuclear Spins in Silicon Carbide. *Physical Review Applied* **2023**, *19*, 034026.
(56) Lekavicius, I.; Myers-Ward, R.; Pennachio, D.; Hajzus, J.; Gaskill, D.; Purdy, A.; Yeats, A.; Brereton, P.; Glaser, E.; Reinecke, T.; Carter, S. Orders of Magnitude Improvement in Coherence of Silicon-Vacancy Ensembles in Isotopically Purified 4H-SiC. *PRX Quantum* **2022**, *3*, 010343.
(57) Marcks, J. C.; Pingault, B.; Zhang, J.; Zeledon, C.; Heremans, F. J.; Awschalom, D. D. Nuclear Spin Engineering for Quantum Information Science. *J. Mater. Res.* **2025**, *40*, 1433−1448.
(58) Kuate Defo, R.; Zhang, X.; Bracher, D.; Kim, G.; Hu, E.; Kaxiras, E. Energetics and Kinetics of Vacancy Defects in 4H-SiC. *Phys. Rev. B* **2018**, *98*, 104103.

Downloaded from http://pubs.acs.org/nalefd/article-pdf/26/28/9143/6583010?/acs.nanolett.6c01807.pdf by TU DELFT user on 06 August 2026

https://doi.org/10.1021/acs.nanolett.6c01807
Nano Lett. 2026, 26, 9143−9150